

Search for a liquid-liquid critical point in models of silica

Erik Lascaris,¹ Mahin Hemmati,² Sergey V. Buldyrev,³ H. Eugene Stanley,¹ and C. Austen Angell²

¹*Center for Polymer Studies and Department of Physics, Boston University, Boston, MA 02215 USA*

²*Department of Chemistry and Biochemistry, Arizona State University, Tempe, AZ 85287 USA*

³*Department of Physics, Yeshiva University, 500 West 185th Street, New York, NY 10033 USA*

(Dated: 12 February 2014)

Previous research has indicated the possible existence of a liquid-liquid critical point (LLCP) in models of silica at high pressure. To clarify this interesting question we run extended molecular dynamics simulations of two different silica models (WAC and BKS) and perform a detailed analysis of the liquid at temperatures much lower than those previously simulated. We find no LLCP in either model within the accessible temperature range, although it is closely approached in the case of the WAC potential near 4000 K and 5 GPa. Comparing our results with those obtained for other tetrahedral liquids, and relating the average Si-O-Si bond angle and liquid density at the model glass temperature to those of the ice-like β -cristobalite structure, we conclude that the absence of a critical point can be attributed to insufficient “stiffness” in the bond angle. We hypothesize that a modification of the potential function to mildly favor larger average bond angles will generate a LLCP in a temperature range that is accessible to simulation. The tendency to crystallize in these models is extremely weak in the pressure range studied, although this tendency will undoubtedly increase with increasing stiffness.

I. INTRODUCTION

Silica (SiO_2) is one of the most important and widely used materials in today’s world. One could say that the fact of its ubiquity is as clear as window glass. Because silica is an excellent insulator and can be easily created through thermal oxidation of the silicon substrate, SiO_2 is also the insulator of choice in the semiconductor industry. Optical fibers made from pure silica are widely used by the telecommunications industry and, because silica and silicates make up over 90% of the Earth’s crust, SiO_2 plays a major role in the geosciences.

Liquid silica is the extreme case of a “strong” liquid. When cooled, its viscosity approaches the glass transition slowly, following the Arrhenius law $\log \eta \propto 1/T$. In contrast, the so-called “fragile” liquids reach this glass transition far more quickly. Glasses rich in silica, but modified by other oxides to lower their viscosities, are “strong” liquids that have slow vitrification so are preferred by glassblowers who need time to work their magic.

Simulations have indicated that liquid silica does not behave like a strong liquid for all temperatures, however. Using the BKS model [1] (see Appendix A), Vollmayr *et al.* found that at very high temperatures the diffusion greatly deviates from the Arrhenius law (and thus behaves like a fragile liquid), and that the temperature-dependence of the diffusion better fits the Vogel-Fulcher law [2]. It was later shown by Horbach and Kob [3] that the temperature-dependence can also be fitted well by a power law of the shape $D \propto (T - T_{\text{MCT}})^\gamma$ in which the exponent γ is close to 2.1 (compared to 1.4 for water) and $T_{\text{MCT}} \approx 3330$ K. This temperature dependence is often found in simple liquids and has been described in terms of mode-coupling theory (MCT) [4, 5]. A deviation from the Arrhenius law has also been measured in other models of silica [6], and small deviations from a pure Arrhenius law were found for the viscosity

in experimental data [7, 8]. This transition from fragile to strong upon cooling (often called the “fragile-to-strong crossover”) has also been found in simulations of other tetrahedral liquids, such as BeF_2 [9], silicon [10, 11], and water [12–14]. This phenomenon is not restricted to tetrahedral liquids, however. For example, it has been proposed that the fragile-to-strong crossover might be a behavior common to all metallic glass-forming liquids [15, 16].

In addition to the fragile-to-strong crossover, it has been proposed that liquid silica also has a liquid-liquid critical point (LLCP) [17–19] much like that proposed for liquid water [20]. These phenomena may be related. It was recently shown that in analog plastic crystal systems many strong glass-formers are accompanied by a singularity (a lambda-type order-disorder transition) at high temperatures, and that in silica this singularity could be a LLCP [19]. If that is the case, the critical MCT temperature T_{MCT} should lie close to the critical temperature of the LLCP. The fragile-to-strong crossover arises simultaneously with a large increase of the isobaric heat capacity C_P . If a LLCP exists in silica, this heat capacity maximum should originate from the LLCP. The discovery of a LLCP in liquid silica would thus provide a unifying thermodynamic explanation for the behavior of liquid silica.

II. METHODS

We consider here two different models of silica, the BKS model by van Beest *et al.* [1] and the WAC model (also known as the TRIM model for silica) introduced by Woodcock *et al.* [21]. Both models represent SiO_2 as a simple 1:2 mixture of Si ions and O ions, i.e., without any explicit bonds. One difference between the two models is that WAC uses full formal charges while in

BKS partial charges are used. For a detailed description of both models, see Appendix A.

We do all simulations using Gromacs 4.6.1 [22], with $N = 1500$ ions, using the Ewald sum (PME) for electrostatics, and the v-rescale thermostat [23] to keep the temperature constant. Most simulations are done in the constant-volume/constant-temperature (NVT) ensemble. For the few constant-pressure (NPT) simulations we use the Parrinello-Rahman barostat. For most of the simulations we use a time step of 1 fs, but at very low temperatures we increase the time step to 4 fs to speed up the simulations to approximately 250 ns/day. We carefully check the temperatures below which the 4 fs time step gives the same results as the 1 fs time step and do not include any 4 fs data that lead to a small difference in pressure, energy, or diffusion.

As a measure of the equilibration time, we define τ as the time at which $\sqrt{\langle r_O(t)^2 \rangle} = 0.56$ nm, i.e., the average time it requires for an O ion to move twice its diameter of 0.28 nm. Most simulations run for over 10τ , well beyond the time necessary for the system to reach equilibration.

III. ISOCHORES

The most direct method of locating a critical point is to calculate the pressure P as a function of temperature T along different isochores. In a PT -diagram the isochores cross within the coexistence region and at the critical point. At those state points (at a given P and T) the system is a combination of two different phases with different densities. One can also locate a critical point by plotting the isotherms in a PV -diagram in order to determine the region in which the slope of the isotherms becomes zero (critical point) or negative (coexistence region). Because it is easier to determine whether two lines are crossing than whether a curve is flat, we study the isochores. Figure 1 shows the PT -diagrams with the isochores of BKS and WAC.

Both diagrams are similar. There is a clear density anomaly to the left of the temperature of maximum density (TMD), and if we raise the temperature by approximately 4000 K then the BKS isochores match those of WAC reasonably well. Thus, based on the isochores in Fig. 1, one could say that BKS and WAC are very similar systems, and that they mainly differ in a shift of temperature.

At very low P and high T the liquid phase is bound by the liquid-gas (or liquid-vacuum) spinodal, and lowering P below the spinodal leads to spontaneous bubble formation. At very low T the liquid becomes a glass, and the diffusion coefficient drops rapidly. Because the time it takes to equilibrate the system is inversely proportional to the rate of diffusion, simulations require too much time once the oxygen diffusion D_O drops below $\sim 10^{-8}$ cm²/s, which is where the isochores stop in Fig. 1. For both models this limit is reached at a higher temperature for low P than for high P . This is caused by the diffusion anomaly

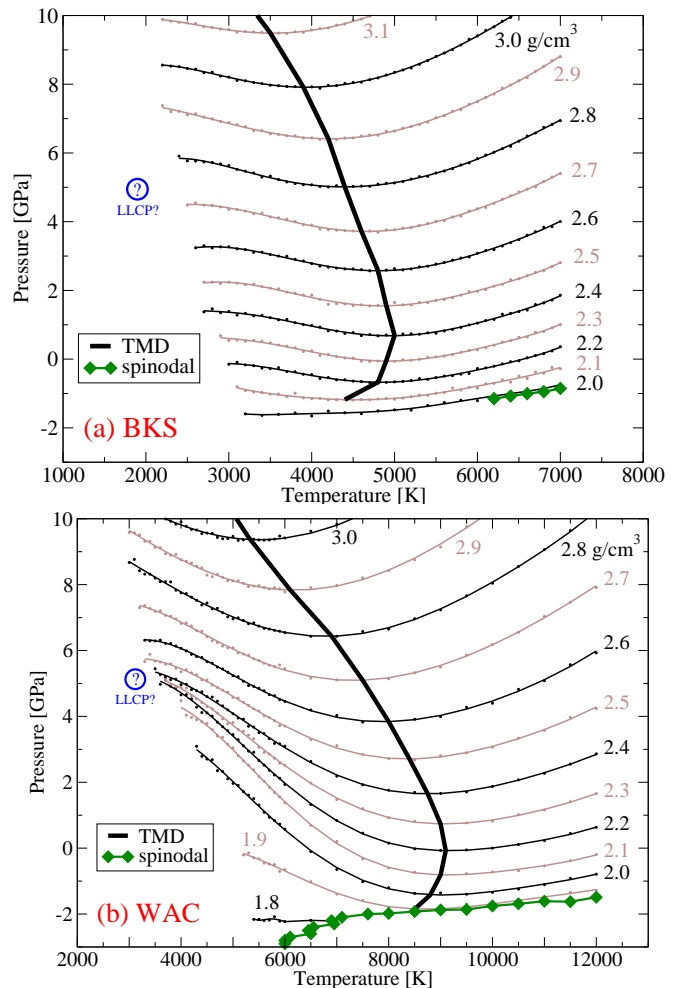


FIG. 1. Isochores of liquid BKS silica (panel a) and liquid WAC silica (panel b). Thin black/brown lines are the isochores, the temperature of maximum density (TMD) is indicated by a thick black line, and green diamonds indicate part of the liquid-vacuum spinodal. Question marks indicate the approximate locations where a LLCP has been predicted by previous studies [18, 19]. The location of a LLCP can be identified by where the isochores cross. It seems a LLCP in BKS is unlikely, as the isochores do not approach each other. The isochores in WAC do approach each other, and might converge at the predicted point. However, at low temperatures the isochores near 2.3 g/cm³ obtain a negative curvature. If this curvature becomes more negative as T goes down, then it is possible that the isochores will not cross below 3500 K. We conclude that for the temperatures currently accessible, the isochores alone are insufficient to demonstrate a LLCP in WAC.

(an increase in P leads to an *increase* in diffusion), which is present in both BKS and WAC.

Based on the fitting and extrapolation of data, previous studies have predicted a liquid-liquid critical point (LLCP) in both WAC and BKS [18]. With the increase in computing power, and using the techniques to speed up the simulations discussed in Sec. II, we are able to obtain data at lower temperatures than was previously possible.

Our results for BKS (Fig. 1a) show that for $T > 2500$ K the isochores are nearly parallel, and therefore a LLCP in BKS is very unlikely. On the other hand, the isochores of the WAC model (Fig. 1b) show a more interesting behavior in that they clearly approach one another at low T in the vicinity of $P \approx 5$ GPa.

If we only consider the WAC isochores above 4000 K, then extrapolation would predict that the isochores cross around 3500 K and 5 GPa. However, below 4000 K we see that the isochores are starting to display a negative curvature in the PT -plane. This signals an approach to a density minimum, which is the low- T limit of the density anomaly region. The negative curvature makes it hard to perform an extrapolation that convincingly shows that the isochores cross at lower T . We can therefore only conclude that (for the temperatures currently accessible) the isochores are insufficient to prove or disprove the existence of a LLCP in WAC.

IV. RESPONSE FUNCTIONS

Upon approaching a critical point, the response functions should diverge. Although true divergence occurs only in the thermodynamic limit $N \rightarrow \infty$, a large maximum should still be visible in response functions such as the isothermal compressibility K_T and the isobaric heat capacity C_P even when the box size is relatively small. Calculations using the Ising model and finite size scaling techniques applied to simulation results have shown that (for sufficiently large boxes) the location of the critical point is very close to where both K_T and C_P reach their global maximum [24, 25]. If a LLCP truly exists in WAC, then the PT -diagrams of C_P and K_T should show a large C_P maximum close to where K_T has a maximum—exactly where the isochores come together and where the LLCP has been predicted to be.

Figure 2 shows four response functions for WAC: (a) the isothermal compressibility K_T , (b) the isobaric heat capacity C_P , (c) the isobaric thermal expansivity α_P , and (d) the isochoric heat capacity C_V . These have been obtained using NVT simulations together with the smooth surface technique described in Appendix B. To check the results generated by this technique, we determine whether the response functions satisfy the thermodynamic relation $VT\alpha_P^2/K_T + C_V - C_P = 0$. Because of statistical errors in the data we find slight deviations from zero, but these are less than 1 J/(mol K) in magnitude.

The compressibility K_T in Fig. 2a shows a clear global maximum near $P \approx 5$ GPa and $T \approx 4000$ K, because this is where the isochores in Fig. 1b are the closest together in terms of pressure. It is quite likely that below 4000 K this maximum increases further. If WAC has a LLCP then C_P should also have a maximum in that vicinity. However, Fig. 2b shows that this is not the case. There is clear global C_P maximum, but it is located near $P \approx 1$ GPa and $T \approx 6000$ K, which is far from the global K_T

maximum. Therefore, based on the response functions, we conclude that WAC does not have a LLCP.

The isobaric thermal expansivity α_P (Fig. 2c) has a global minimum between the global maxima of C_P and K_T (Figs. 2a,b). This should come as no surprise, since $C_P \propto \langle \Delta S \rangle^2$ arises from fluctuations in entropy and $K_T \propto \langle \Delta V \rangle^2$ from volume fluctuations, while the expansivity $\alpha_P \propto \langle \Delta S \rangle \langle \Delta V \rangle$ arises from a combination of both. It is therefore likely the mechanism that is responsible for the C_P maximum is the same mechanism that causes the K_T maximum and the α_P minimum.

Although Fig. 1a already makes clear that a LLCP in BKS silica is quite unlikely, it is worth mentioning that the C_P of BKS displays exactly the same behavior as the C_P of WAC. The PT -diagram of C_P for BKS strongly resembles Fig. 2b of WAC. Instead of showing the same figure twice, we present in Fig. 3 the BKS heat capacity C_P as a function of T for five different pressures. We obtain this figure by performing 10 cooling/heating cycles at a rate of 1000 K/ns. At a certain temperature the heating and cooling curves separate, and below this temperature the liquid is no longer in equilibrium. The figure clearly shows that there is a C_P maximum in BKS that decreases upon increasing the pressure—exactly the same phenomenon as in WAC.

V. DISCUSSION

We fail to find a liquid-liquid critical point (LLCP) in either BKS or WAC silica. The isochores of BKS, which are the most direct indicators of criticality in a physical system, fail to converge into a critical point. In the case of WAC we cannot conclude anything from the isochores, but an analysis of the global extrema of the response functions indicates that there is no LLCP in WAC because the global C_P maximum and the global K_T maximum are significantly separated in the PT -plane.

Liquid silica forms a tetrahedral network of bonds, and below we will show that the lack of a LLCP is related to the openness of this network structure, which in turn is related to the stiffness of the inter-tetrahedral bond angles. In addition we will argue that criticality in WAC could be achieved with an adaptation of the pair potential.

The occurrence of a LLCP requires two competing liquid structures that can be in a (meta-stable) equilibrium with each other. In the case of a tetrahedral network-forming liquid the two relevant structures are usually: (i) a high-density collapsed structure that is highly diffusive, and (ii) a low-density open network structure that is more rigid, i.e., one that is still a liquid but less diffusive and more structured. Because the high-density structure occupies a smaller volume but has higher entropy (more disorder), the competition between these two structures is accompanied by a region with a density anomaly: $\alpha_P \propto \langle \Delta S \rangle \langle \Delta V \rangle < 0$.

The high-density structure is very stable and is the

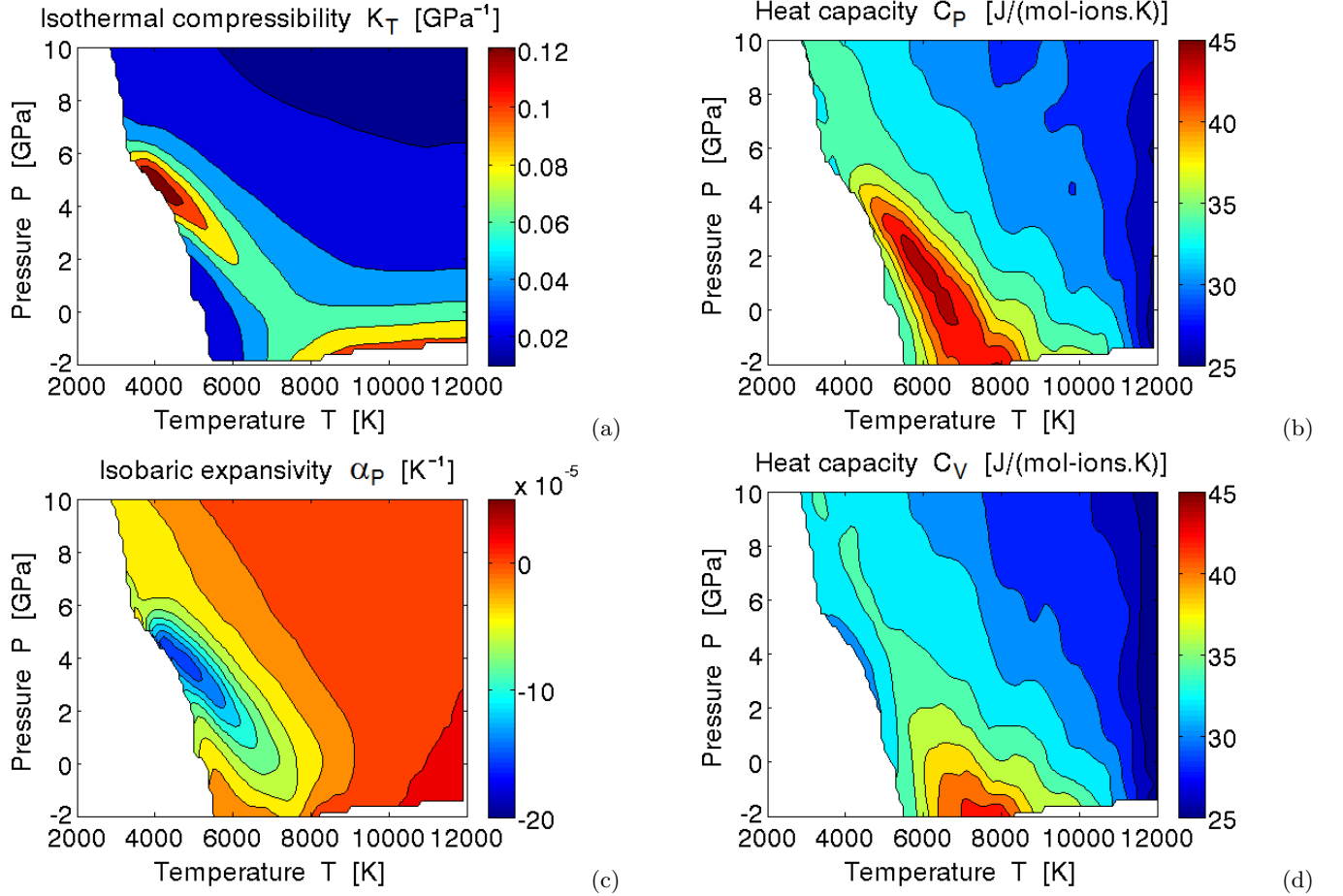


FIG. 2. Response functions of WAC. (a) The isothermal compressibility K_T is consistent with a LLCP near 5 GPa, 4000 K because near that point K_T has a global maximum. (b) The isobaric heat capacity C_P , however, has a global maximum around 1 GPa and 6000 K, far away from where K_T has its global maximum. This is inconsistent with the LLCP hypothesis. (c) The isobaric thermal expansivity α_P has its global minimum in between the global maxima of K_T and C_P . The contour line where $\alpha_P = 0$ corresponds to the location of the TMD. (d) The isochoric heat capacity C_V has its global maximum the furthest away from the global K_T maximum.

dominant structure at high temperatures, but the low-density structure requires a more delicate balance of forces in order to be stable. If the bonds in the liquid are too flexible, the liquid collapses into the high-density structure. On the other hand, if the bonds are too rigid the liquid can no longer flow and ceases to be a fluid.

There are two previous studies that address this situation. The 2006 study of Molinero *et al.* [26] shows how reducing the three-body repulsion parameter λ in the Stillinger-Weber potential [27] (which controls the bond angle stiffness) causes the first order liquid-liquid phase transition of silicon ($\lambda = 21$) to disappear at $P = 0$ when $\lambda < 20.25$ (see Fig. 4). This transition occurs between a low-density liquid and a high-density liquid, where both liquids are metastable with respect to the diamond cubic (dc) crystal. Crystallization to the dc crystal always occurs from the low-density liquid. When $\lambda > 21.5$ crystallization happens so fast that it is no longer possible to accurately determine the temperature T_{LL} at which the

phase transition occurs for $P = 0$.

Simulations of the Stillinger-Weber model indicate that the LLCP for $\lambda = 21$ is located at -0.60 GPa and 1120 K [28]. Since each value of λ defines a unique system with a unique critical pressure, the vanishing of the liquid-liquid transition at $\lambda < 20.25$ implies that this is the λ value for which the LLCP is at $P = 0$. Isochore-crossing studies conducted elsewhere [29] show that this is indeed the case, with $T_c \approx 700$ K for $P_c = 0$. It is clear that decreasing λ means decreasing the tetrahedrality and increasing density. When $\lambda < 20.25$ the LLCP shifts to positive pressures, and therefore the phase transition line can no longer be seen in Fig. 4, as it only considers $P = 0$. We thus lack the information to determine exactly for which λ there is no LLCP at *any* pressure, but it is certain that this happens at some value $\lambda > 0$, since in the most extreme case of $\lambda = 0$ we are left with a simple Lennard-Jones-like model that has no LLCP.

That weakening the tetrahedrality (i.e., making the

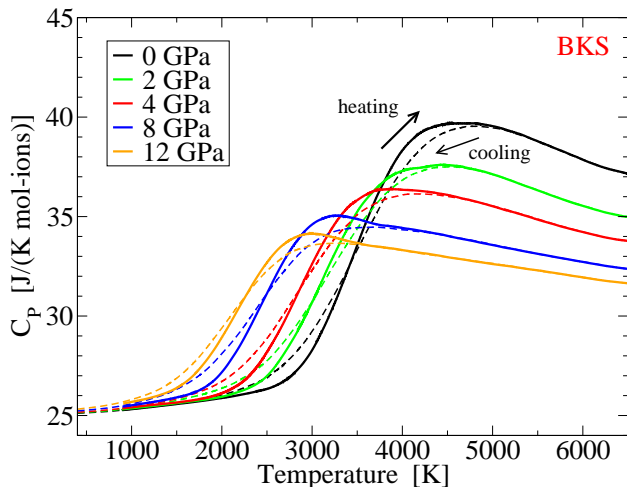


FIG. 3. The heat capacity of BKS shows the same behavior as WAC: a large C_P maximum at low pressures, which decreases when the pressure is increased. If there were a LLCPP near 5 GPa and low T , then we would expect to see C_P increase instead. The curves in this plot are calculated by repeatedly cooling and heating the liquid at a rate of 1000 K/ns and at constant pressure. No crystallization occurs during this process; the liquid becomes an amorphous solid at low T instead. The system is no longer in equilibrium where the cooling and heating curves split, and here the values of C_P are only approximate.

tetrahedral bonds more flexible) leads to the removal of a LLCPP, was also shown in 2012 by Tu and co-authors using a different monatomic model [30]. The Hamiltonian of this model includes a term that lowers the energy when particles are aligned along near-tetrahedral angles and thus favors a diamond cubic ground state. The study of Ref. [30] considers two versions: one that allows broad flexibility of the inter-tetrahedral bond angles (leading to weak tetrahedrality), and another in which the bond angle is more constrained (giving rise to strong tetrahedrality).

The behavior for strong tetrahedrality is shown in Fig. 5, and we see that the isochores converge into a critical point. If the tetrahedrality is weakened slightly, then the isochores separate, the LLCPP disappears, and the diagram starts to resemble that of Fig. 1b for WAC. It should be mentioned that a separation of the global C_P and K_T maxima also occurs in the weak tetrahedrality version (as is the case for WAC), while the C_P and K_T maxima are close together and near the LLCPP in the strong version of the model.

Both of these earlier studies show that the occurrence of a LLCPP becomes less likely when the parameters controlling tetrahedrality are weakened. Unfortunately, the BKS and WAC models do not have an explicit parameter that controls tetrahedrality, such as the parameter λ in the Stillinger-Weber model. In this model there is a direct relation between the value of λ and the tetrahedrality of the liquid measured by the orientational order pa-

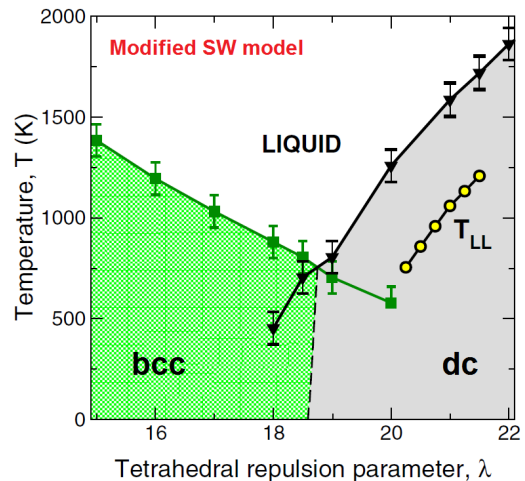


FIG. 4. Phase diagram of the modified Stillinger-Weber potential in terms of the tetrahedral repulsion parameter λ and temperature T , at zero pressure (figure adapted from [26]). The black triangles indicate the melting line of the diamond cubic (dc) crystal, while the green squares denote the melting line of the bcc crystal. The dashed line separates the dc and bcc regions. Yellow circles indicate the transition temperature T_{LL} at which the liquid-liquid phase transition line crosses the $P = 0$ isobar for that particular value of λ . Silicon is represented by $\lambda = 21$ and has a liquid-liquid critical point at -0.60 GPa [28], and therefore all LLCPPs for $\lambda > 20.25$ lie at negative pressures (there is a LLCPP for each value of λ). For $\lambda < 20.25$ the LLCPPs are at positive pressures and therefore the phase transition line can no longer be seen in this diagram. When λ is large the system easily crystallizes, and therefore the phase transition line at $P = 0$ can no longer be accurately located when $\lambda > 21.5$.

rameter q as defined by Errington and Debenedetti [31]. This parameter is constructed such that its average value $\langle q \rangle$ will equal zero if all atoms are randomly distributed within the liquid, while $q = 1$ for each atom within a perfect tetrahedral network (such as in a cubic diamond lattice). For silica the situation is more complicated. It is not immediately clear how to define the tetrahedrality of a system that consists of two types of atoms. One way would be to find for each Si atom its four nearest neighboring Si atoms and compute $\langle q \rangle$ for this subset of atoms. However, this measure would completely ignore the positions of the O atoms which form ionic bridges between the Si atoms. Since the O-Si-O bond angle deviates very little from the perfect tetrahedral angle of 109° [2], it makes sense to focus on the inter-tetrahedral Si-O-Si bond angle instead. It is commonly agreed upon that structures such as diamond cubic have maximum tetrahedrality, and for silica this corresponds to a system where all Si-O-Si bond angles are equal to 180° (such as β -cristobalite). How much the inter-tetrahedral Si-O-Si bond angles differ from 180° can thus be employed as a measure of the tetrahedrality, and we have therefore calculated this bond angle distribution for both BKS and WAC. The location of the maximum in the Si-O-Si bond

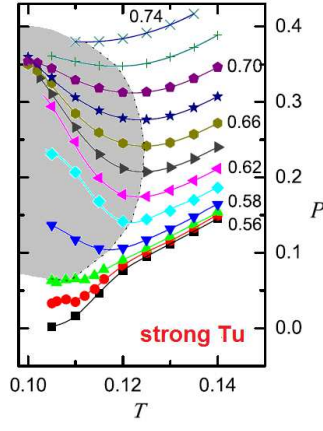


FIG. 5. Isochores of the Tu model for the strong tetrahedrality version, which has a LLCP (figure adapted from Ref. [30]). Gray area indicates the density anomaly region. By reducing the tetrahedrality, the Tu model can be smoothly changed into the weak tetrahedrality version, which does not have a LLCP. The isochores of WAC (Fig. 1b) show no LLCP but closely resembles that of the strong Tu model. We can interpret this as that WAC is *close* to having a LLCP, but not close enough. If we were to enhance the tetrahedrality of WAC, it is likely a LLCP would appear.

angle distribution (i.e., the most probable angle) is a parameter that one could use to quantify the tetrahedrality. If we denote the most probable angle at the lowest accessible temperature (T_g) as θ_{\max} , then the tetrahedrality parameter t can be defined as $t \equiv \theta_{\max}/180^\circ$, where $0 < t < 1$. Since the “openness” of the structure will increase with the average Si-O-Si angle, one could also define the tetrahedrality using the volume ratio, i.e., $t \equiv V^*/V_{\text{dc}}$, which would require much less effort to calculate. Here V_{dc} is the volume of the perfect diamond cubic and V^* is the system volume at some corresponding state, for instance at the TMD (which is less arbitrary than T_g).

Let us consider the angular relations and the mechanical forces that determine them in more detail. In terms of the familiar ball-and-stick model, the Si-O-Si bond could be represented by two sticks connected at the oxygen atom, with a spring in between the sticks. This spring constrains the bond angle to some preferred bond angle θ_0 , while the value of its spring constant k_2 (the *stiffness*) dictates how flexible the bond angle is. From the bond angle probability distribution $\mathcal{P}(\theta)$, it is possible to estimate the values of the preferred bond angle θ_0 and the bond angle stiffness k_2 .

To extract the Si-O-Si bond angles from the data, we consider each O ion together with its two nearest Si neighbors and calculate the angle between the two Si-O bonds. In Fig. 6 we show the resulting probability distributions $\mathcal{P}(\theta)$ of the Si-O-Si angle θ for BKS and WAC at zero pressure. These curves have been measured before in previous studies [2, 6] but with less detail. As the temperature decreases, the width of the distribution

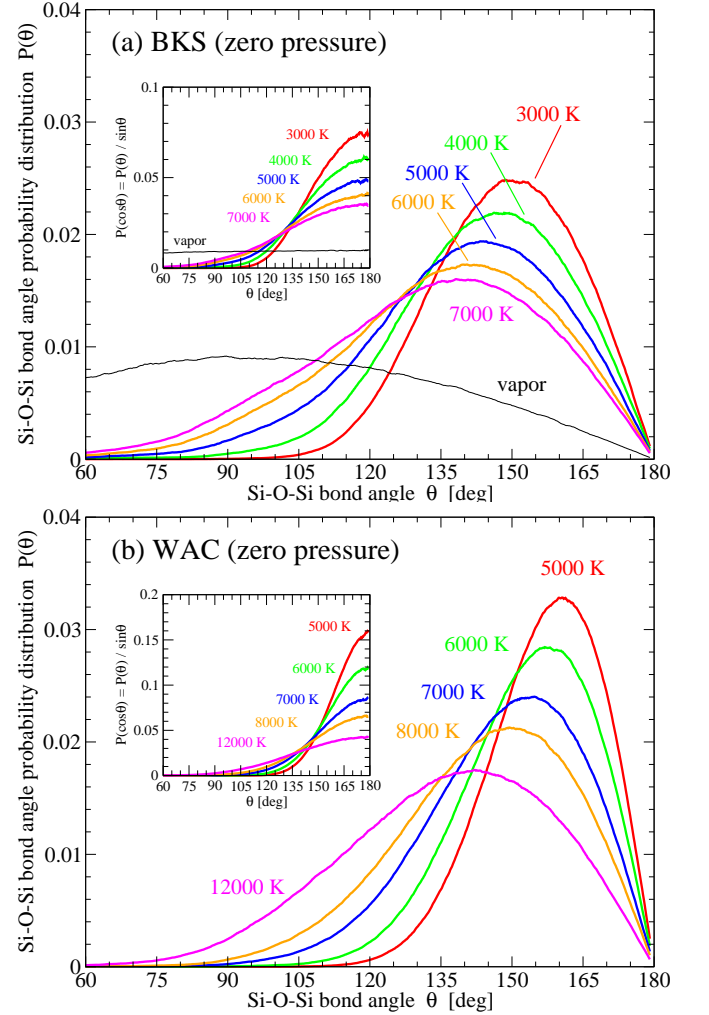


FIG. 6. Probability distribution of the Si-O-Si bond angle $\mathcal{P}(\theta)$ in liquid silica for (a) the BKS model and (b) the WAC model. As T goes down, the most probable angle moves closer to 180° while simultaneously the width of the distribution decreases. The first phenomenon causes the liquid to expand upon cooling, while a reduction in width means that the bonds become stiffer, which leads to a decrease in diffusion. Both phenomena are related (see below) and are much stronger for WAC than for BKS. Instead of $\mathcal{P}(\theta)$ it is better to consider $\mathcal{P}(\cos \theta) = \mathcal{P}(\theta)/\sin \theta$, since a completely random distribution such as in the vapor has $\mathcal{P}(\theta) \propto \sin \theta$ while $\mathcal{P}(\cos \theta)$ is uniform (see inset of panel a). For both models and all temperatures $\mathcal{P}(\cos \theta)$ resembles a normal distribution with mean 180° . This indicates that the preferred angle is in fact 180° , and that the width of $\mathcal{P}(\cos \theta)$ determines both the location of the peak in $\mathcal{P}(\theta)$ as well as its width.

decreases and the maximum shifts toward 180° . This implies that the liquid becomes more structured and stiffer. This is to be expected, since at a high temperatures there are more thermal fluctuations and therefore $\mathcal{P}(\theta)$ has a broader distribution.

Plotting $\mathcal{P}(\theta)$ may not be the best way of presenting the bond angle distribution, as this distribution is bi-

ased toward 90° angles. This is particularly clear from the distribution of the vapor (the thin black line in Fig. 6a). The ions in the vapor have no preferred position with respect to their neighbors, yet $\mathcal{P}(\theta)$ is not uniform but proportional to $\sin \theta$. This is related to the fact that the infinitesimal area element of the unit sphere is $dA = \sin \theta d\theta d\phi$ rather than $d\theta d\phi$. As $\theta \rightarrow 180^\circ$ the area element dA approaches zero, and therefore $\mathcal{P}(\theta) = 0$ at $\theta = 180^\circ$. Instead of $\mathcal{P}(\theta)$ it is better to consider the probability distribution $\mathcal{P}(\cos \theta) = \mathcal{P}(\theta)/\sin \theta$, as is shown in the insets of Fig. 6. The $\mathcal{P}(\cos \theta)$ distribution of the vapor is a uniform distribution (inset of Fig. 6a). For the liquid, the distribution $\mathcal{P}(\cos \theta)$ is approximately a normal distribution with its mean at $\theta_0 = 180^\circ$. Evidently the most probable inter-tetrahedral angle (the location of the $\mathcal{P}(\theta)$ -peak) is purely an effect of the width of this normal distribution combined with the fact that $dA \propto \sin \theta$.

It is possible to interpret the bond angle distribution in terms of an effective potential $U_{\text{eff}}(\theta)$, assuming that $\mathcal{P}(\cos \theta) \propto \exp[-U_{\text{eff}}(\theta)/k_B T]$. When the effective potential is harmonic, i.e. $U_{\text{eff}} = \frac{1}{2}k_2(\theta - \theta_0)^2$, the resulting probability distribution is a normal distribution with mean θ_0 and a width that depends on temperature T and stiffness k_2 . In general the effective potential will not be perfectly harmonic and includes anharmonic terms. Because $\cos \theta$ is an even function about $\theta = 180^\circ$, it is required that $\mathcal{P}(\cos \theta)$ is as well, and therefore also $U_{\text{eff}}(\theta)$. Consequently, the leading-order anharmonic term in $U_{\text{eff}}(\theta)$ is of the fourth order. The Si-O-Si bond angle distribution can thus be described by

$$\mathcal{P}(\theta) = A \sin \theta \exp[-U_{\text{eff}}(\theta)/k_B T] \quad (1)$$

with U_{eff} a Taylor series about the mean angle $\theta_0 = 180^\circ$,

$$U_{\text{eff}}(\theta) = \frac{1}{2}k_2(\theta - \theta_0)^2 + \frac{1}{4!}k_4(\theta - \theta_0)^4 + \dots \quad (2)$$

Here A is a temperature-dependent normalization constant that ensures that the total probability $\int \mathcal{P}(\theta) d\theta = \int \mathcal{P}(\cos \theta) d\cos \theta$ is equal to one, and k_B is the Boltzmann constant.

The probability distributions of Fig. 6 can be fitted quite well with Eqs. 1 and 2, even when the sixth power and higher-order terms are ignored. The resulting values for the stiffness k_2 are shown in Fig. 7. It is immediately clear that WAC is far more rigid than BKS. For BKS the stiffness does not vary much with temperature, while increasing the pressure makes the bonds slightly less stiff. The same is true for WAC at high T , but below 5 GPa the stiffness shows an increase when the liquid is cooled. This increase is exactly where C_P has its maximum in Fig. 2b, and thus we may argue that the increase in C_P is due to a structural change, namely the stiffening of the tetrahedral network.

From the isochores in Fig. 1b it is clear that WAC is very close to having a LLCP. If we compare the results of previous studies done on tetrahedral liquids [26, 30] with our results for BKS and WAC, then we see that

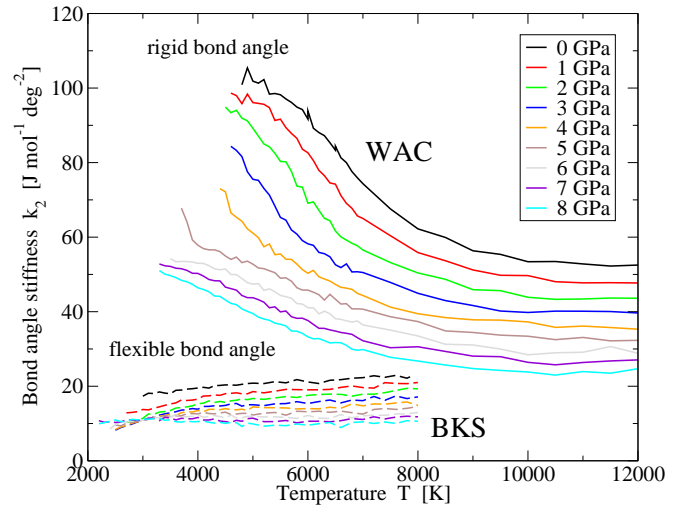


FIG. 7. Stiffness of the Si-O-Si bond angle for both WAC (solid lines, top) and BKS (dashed lines, bottom). For both models the stiffness k_2 goes down with increasing pressure. It is clear that BKS has more flexible bonds (small k_2), and that WAC is more rigid (large k_2) and therefore “more tetrahedral”. In addition WAC shows a transition at low T for $P \leq 5$ GPa to a state with an even higher stiffness.

the tetrahedrality of BKS is far too small (i.e., the inter-tetrahedral bond angles are not sufficiently stiff) to have a LLCP, and that WAC is close, but not close enough. However, it might be possible to make a small change to the WAC potential to enhance its tetrahedrality. One simple way to achieve this is to add a repulsive term similar to the three-body interaction of the Stillinger-Weber model. This term should penalize any Si-O-Si configuration with an angle less than 180° with a repulsive energy determined by the intensity parameter λ and the size of the deviation. The λ value associated with this interaction should be carefully chosen. Based on Fig. 7 we estimate that the modified WAC model should have a LLCP if the stiffness k_2 reaches a value around 60–80 J/(mol deg²) at high T for zero pressure. It would be interesting to see at what value of k_2 this criticality is introduced, and if this value is the same across other tetrahedral models as well. We encourage other researchers to explore this idea of modifying WAC and verify our hypothesis that WAC can be pushed into criticality by stiffening the Si-O-Si bond angles.

VI. CONCLUSION

Although it has been suggested, based on a combination of simulation and theoretical considerations [18], that both BKS and WAC have LLCPs at temperatures beyond the accessible simulation range, our study suggests that neither BKS nor WAC can reach a critical point. We have compared our results to those of other tetrahedral models [26, 30], analyzed the bond angle distributions,

and conclude that the lack of a LLCP in both BKS and WAC is due to a lack of stiffness in the inter-tetrahedral Si-O-Si bond angles. WAC is close to criticality, but BKS shows little sign of a LLCP, and since the latter is considered to be the more realistic model for experimental silica, we expect that no LLCP occurs in real silica either.

However, this does not mean that manifestations of criticality can never be observed. As Chatterjee and Debenedetti [32] have shown theoretically, even a weak tendency towards criticality (as in BKS) can be amplified into a liquid-liquid phase separation in a binary system. Indeed this notion has been exploited elsewhere [33] to interpret the (much-studied [34–40] but incompletely understood) splitting out of an almost pure SiO₂ phase from such simple systems as the Na₂O-SiO₂ and Li₂O-SiO₂ binary glasses during supercooling.

VII. ACKNOWLEDGMENTS

We would like to thank P. Debenedetti, V. Molinero, H. Aragão, and C. Calero for the many valuable discussions. EL and HES thank the National Science Foundation (NSF) Chemistry Division for support (Grant No. CHE 12-13217) SVB thanks the Dr. Bernard W. Gamson Computational Science Center at Yeshiva College for support. CAA acknowledges the support of this research through the the National Science Foundation (NSF) experimental chemistry program under collaborative Grant no. CHE 12-13265.

Appendix A: WAC and BKS silica

One of the simplest models for silica is the WAC model introduced by L. V. Woodcock, C. A. Angell, and P. Cheeseman [21]. The model is sometimes also known as the Transferable Ion Model (TRIM) because its potential is rather general and can also be used to model other ionic liquids [41]. In the WAC model, the material consists of a 1:2 mixture of Si⁺⁴ and O⁻² ions, without any explicit bonds. Apart from the electrostatic force, the ions also interact with each other via an exponential term:

$$U_{\text{WAC}}(r_{ij}) \equiv \frac{1}{4\pi\epsilon_0} \frac{z_i z_j e^2}{r_{ij}} + a_{ij} \left(1 + \frac{z_i}{n_i} + \frac{z_j}{n_j} \right) \times \exp[B_{ij}(\sigma_i + \sigma_j - r_{ij})] \quad (\text{A1})$$

Here the subscripts $i, j \in \text{Si, O}$ indicate the species of the two ions involved, z_i the charge of each ion ($z_{\text{Si}} = +4$, $z_{\text{O}} = -2$), $n_{\text{Si}} = n_{\text{O}} = 8$ the number of outer shell electrons, and σ_i the size of each ion ($\sigma_{\text{Si}} = 0.1310$ nm, $\sigma_{\text{O}} = 0.1420$ nm). For WAC silica the parameters a_{ij} and B_{ij} are the same for all pairs: $a_{ij} = 0.19$ perg ≈ 11.44 kJ/mol and $B_{ij} = 34.48$ nm⁻¹ [41]. The potential

can also be written as

$$U_{\text{WAC}}(r_{ij}) = \frac{1}{4\pi\epsilon_0} \frac{q_i q_j}{r_{ij}} + A_{ij} \exp(-B_{ij} r_{ij}), \quad (\text{A2})$$

with $A_{\text{SiSi}} = 1.917991469 \times 10^5$ kJ/mol, $A_{\text{SiO}} = 1.751644217 \times 10^5$ kJ/mol, and $A_{\text{OO}} = 1.023823519 \times 10^5$ kJ/mol.

The second model that we consider here is BKS. Currently one of the most popular models, the BKS model was introduced by B. W. H. van Beest, G. J. Kramer, and R. A. van Santen [1] and is similar to WAC. Silica is again modeled as a simple 1:2 mixture of Si- and O-ions, without explicit bonds. To produce results that better match experiments and *ab initio* simulations, and to be able to effectively represent screening effects, the charges in BKS are not integer values of e but instead are given by $q_{\text{Si}} = +2.4e$ and $q_{\text{O}} = -1.2e$. In addition to this, the BKS potential also differs from the WAC model in that it includes an attractive r^{-6} term:

$$U_{\text{BKS}}(r_{ij}) \equiv \frac{1}{4\pi\epsilon_0} \frac{q_i q_j}{r_{ij}} + A_{ij} \exp(-B_{ij} r_{ij}) - C_{ij} r_{ij}^{-6}. \quad (\text{A3})$$

In BKS there is no interaction between two Si-ions apart from the electrostatics, i.e. $A_{\text{SiSi}} = B_{\text{SiSi}} = C_{\text{SiSi}} = 0$. The parameters for the Si-O pair are $A_{\text{SiO}} \equiv 18003.7572$ eV, $B_{\text{SiO}} \equiv 4.87318$ Å⁻¹, and $C_{\text{SiO}} \equiv 133.5381$ eV Å⁶. For the O-O interaction, the numbers are $A_{\text{OO}} \equiv 1388.7730$ eV, $B_{\text{OO}} \equiv 2.76$ Å⁻¹, and $C_{\text{OO}} \equiv 175$ eV Å⁶.

Although the BKS model has been quite successful in simulations of quartz and amorphous silica, at temperatures above ~ 5000 K two ions can come very close, causing problems. As $r \rightarrow \infty$ the BKS potential diverges to $-\infty$ and the two ions fuse together—a non-physical phenomenon that is an artifact of the model. One way to solve this issue is by including an additional repulsive term at very small r , e.g., by adding a r^{-30} term [18]. When such a large power is used, however, a small time step is required to prevent large forces, which leads to much slower simulations. Because of this, we instead adjust the BKS potential at small r by adding a second-degree polynomial for $r \leq r_s$. Here r_s is the point at which the original BKS force has an inflection, i.e., where $d^2 F_{\text{BKS}}/dr^2 = -d^3 U_{\text{BKS}}/dr^3 = 0$. We choose the coefficients of the polynomial such that the new potential $U(r)$ has no inflection at $r = r_s$. Adding the polynomial still leads to $U(r) \rightarrow -\infty$ when $r \rightarrow 0$, but increases the height of the energy barrier sufficiently to allow us to simulate the high temperatures we wish to explore. Choosing a short-range correction to BKS has been found to have little effect on the simulation results, and merely prevents the ions from fusing.

To further speed up the simulations, we modify the BKS potential as described by K. Vollmayr, W. Kob, and K. Binder in Ref. [2], and truncate and shift the potential at $r_c = 0.55$ nm. Although this truncation leads to a shift in pressure, it otherwise produces approximately

	Si-O	O-O	units
a_{ij}	$2.678\,430\,850 \times 10^5$	$9.208\,901\,230 \times 10^4$	kJ/mol nm^2
b_{ij}	$-7.343\,377\,221 \times 10^4$	$-4.873\,373\,066 \times 10^4$	kJ/mol nm
c_{ij}	$2.353\,960\,789 \times 10^3$	$7.337\,042\,047 \times 10^3$	kJ/mol
A_{ij}	$1.737\,098\,076 \times 10^6$	$1.339\,961\,920 \times 10^5$	kJ/mol
B_{ij}	48.7318	27.6	nm^{-1}
C_{ij}	$1.288\,446\,484 \times 10^{-2}$	$1.688\,492\,907 \times 10^{-2}$	$\text{nm}^6 \text{kJ/mol}$
$U_{c,ij}$	-0.465 464 470	-0.575 753 031	kJ/mol
r_s	0.139 018 528	0.195 499 453	nm
r_c	0.55	0.55	nm

TABLE I. Parameters of the modified BKS potential of Eq. (A4). Because Si-Si only has the (repulsive) Coulomb interaction, all parameters are zero for Si-Si. One mol here indicates one mol of ions, not one mol of SiO_2 molecules.

the same results [2]. In conclusion, the modified BKS potential we use is given by

$$\begin{aligned}
 U'_{\text{BKS}}(r_{ij}) = & \frac{1}{4\pi\epsilon_0} \frac{q_i q_j}{r_{ij}} \\
 & + \begin{cases} a_{ij} r_{ij}^2 + b_{ij} r_{ij} + c_{ij} - \frac{1}{4\pi\epsilon_0} \frac{q_i q_j}{r_{ij}} & (r_{ij} < r_s) \\
 A_{ij} \exp(-B_{ij} r_{ij}) - C_{ij} r_{ij}^{-6} - U_{c,ij} & (r_s < r_{ij} < r_c) \\
 0 & (r_{ij} > r_c), \end{cases} \quad (\text{A4})
 \end{aligned}$$

with the parameter values for $ij = \text{SiO}$ and $ij = \text{OO}$ listed in Table I. For the Si-Si interaction the potential is $U'_{\text{BKS}}(r_{\text{SiSi}}) = \frac{1}{4\pi\epsilon_0} q_{\text{Si}}^2 / r_{ij}$ and does not involve any cutoffs, apart from the real-space cutoff of the Ewald sum.

Appendix B: Calculation of response functions via surface fits

In order to construct isobaric response functions from a large set of constant-volume (NVT) data, some type of fit or interpolation is needed. For example, to calculate $C_P = (\partial H / \partial T)_P$ we consider the enthalpy H as a function of both P and T and fit the data $[P, T, H]$ with a smooth 3-dimensional surface $H(P, T)$. Abrupt changes in $H(P, T)$ lead to large spikes in its derivative $\partial H / \partial T$, and thus the $H(P, T)$ surface must be smooth if we are to obtain a meaningful C_P . Fitting a surface rather than a curve has the additional advantage that more data is taken into account, resulting in better statistics. An alternative approach is to calculate C_P via fluctuations in

H , but it has been shown [25] that first fitting $H(T)$ and then taking a derivative leads to cleaner results. It is of course easier to calculate C_P by doing constant-pressure (NPT) simulations instead, but then one would have the same problem with calculating C_V . We conclude that we can easily calculate all response functions if we apply a smooth surface fit $f(x, y)$ to a set of 3-dimensional points $z_k(x_k, y_k)$.

Fitting a surface to a set of points means striking a balance between the “smoothness” of the fit and the fitting error induced. One measure of smoothness is the Laplacian $\nabla^2 f$, since a small Laplacian means little change in the slope of $f(x, y)$, and thus a smoother function. Hence, to obtain a smooth surface fit $f(x, y)$ through the data points $z_k(x_k, y_k)$ with $k = 1, 2, \dots, N$, we minimize

$$J = \sum_{k=1}^N w_k [f(x_k, y_k) - z_k]^2 + \iint |\nabla^2 f(x, y)|^2 dx dy. \quad (\text{B1})$$

The weights w_k provide the balance between the smoothness and the fitting error. If we set w_k too low, we obtain a very smooth fitting function $f(x, y)$ that poorly represents the data. If we set w_k too high, the function $f(x, y)$ will go through all the data points but will show large variations. Because large variations in the surface lead to even larger variations in the derivatives, the $H(P, T)$ surface must be very smooth when we calculate the C_P . Fortunately, introducing small fitting errors does not cause problems, because the simulation data already suffers from small statistical errors. If the underlying response function is in fact smooth, then it is possible to use the fitting errors to partially cancel the statistical errors.

Minimization of the functional J in Eq. B1 is not a new concept. For example, the CSAPS function in MATLAB applies a similar minimization scheme to calculate a cubic smoothing spline. As opposed to this MATLAB function, we do not impose the constraint that $f(x, y)$ is a tensor product spline, but instead represent $f(x, y)$ by a set of 100×100 points (x_i, y_j, f_{ij}) placed on a regular grid (x_i, y_j) . Bilinear interpolation is used to estimate the value of $f(x, y)$ between these grid points, and the derivatives and the Laplacian are calculated using finite (central) differences. To compensate for the reduced number of data points near the edges of the domain, we recommend that higher-order differences near the edges be used.

-
- [1] B. W. H. VAN BEEST, G. J. KRAMER, and R. A. VAN SANTEN, *Phys. Rev. Lett.* **64**, 1955 (1990).
[2] K. VOLLMAIR, W. KOB, and K. BINDER, *Phys. Rev. B* **54**, 15808 (1996).
[3] J. HORBACH and W. KOB, *Phys. Rev. B* **60**, 3169 (1999).

- [4] W. GÖTZE, *Liquids, Freezing and the Glass Transition*, in *Proceedings of the Les Houches Summer School of Theoretical Physics, Session LI*, edited by J.-P. HANSEN, D. LEVESQUE, and J. ZINN-JUSTIN, pp. 287–503, North-Holland, Amsterdam, 1991, 1989.

- [5] W. GÖTZE and L. SJÖGREN, *Rep. Prog. Phys.* **55**, 241 (1992).
- [6] M. HEMMATTI and C. A. ANGELL, Comparison of Pair Potential Models for the Simulation of Liquid SiO₂: Thermodynamic, Angular-Distribution, and Diffusional Properties, in *Physics Meets Mineralogy: Condensed Matter Physics in the Geosciences*, edited by H. AOKI, Y. SYONO, and R. J. HEMLEY, chapter 6.1, pp. 325–339, Cambridge University Press, Cambridge, England, 2000.
- [7] K.-U. HESS, D. B. DINGWELL, and E. RÖSSLER, *Chem. Geol.* **128**, 155 (1996).
- [8] E. RÖSSLER, K.-U. HESS, and V. N. NOVIKOV, *J. Non-Cryst. Solids* **223**, 207 (1998).
- [9] C. A. ANGELL, R. D. BRESSEL, M. HEMMATTI, E. J. SARE, and J. C. TUCKER, *Phys. Chem. Chem. Phys.* **2**, 1559 (2000).
- [10] S. SASTRY and C. A. ANGELL, *Nature Mater.* **2**, 739 (2003).
- [11] S. S. ASHWIN, U. V. WAGHMARE, and S. SASTRY, *Phys. Rev. Lett.* **92**, 175701 (2004).
- [12] K. ITO, C. T. MOYNIHAN, and C. A. ANGELL, *Nature* **398**, 492 (1999).
- [13] P. GALLO and M. ROVERE, *J. Chem. Phys.* **137**, 164503 (2012).
- [14] L. XU, P. KUMAR, S. V. BULDYREV, S.-H. CHEN, P. H. POOLE, F. SCIORTINO, and H. E. STANLEY, *Proc. Natl. Acad. Sci. U.S.A.* **102**, 16558 (2005).
- [15] C. ZHANG, L. HU, Y. YUE, and J. C. MAURO, *J. Chem. Phys.* **133**, 014508 (2010).
- [16] K. N. LAD, N. JAKSE, and A. PASTUREL, *J. Chem. Phys.* **136**, 104509 (2012).
- [17] P. H. POOLE, M. HEMMATI, and C. A. ANGELL, *Phys. Rev. Lett.* **79**, 2281 (1997).
- [18] I. SAIKA-VOIVOD, F. SCIORTINO, and P. H. POOLE, *Phys. Rev. E* **63**, 011202 (2000).
- [19] C. A. ANGELL and M. HEMMATI, Glass Transitions and Critical Points in Orientationally Disordered Crystals and Structural Glassformers: (“Strong” Liquids are More Interesting Than We Thought), in *4th International Symposium on Slow Dynamics in Complex Systems*, edited by M. TOKUYAMA and I. OPPENHEIMER, volume 1518, p. 9, AIP Conf. Proc., 2013.
- [20] P. H. POOLE, F. SCIORTINO, U. ESSMANN, and H. E. STANLEY, *Nature* **360**, 324 (1992).
- [21] L. V. WOODCOCK, C. A. ANGELL, and P. CHEESEMAN, *J. Chem. Phys.* **65**, 1565 (1976).
- [22] B. HESS, C. KUTZNER, D. VAN DER SPOEL, and E. LINDAHL, *J. Chem. Theory Comp.* **4**, 435 (2008).
- [23] G. BUSSI, D. DONADIO, and M. PARRINELLO, *J. Chem. Phys.* **126**, 014101 (2007).
- [24] T. A. KESSELRING, E. LASCARIS, G. FRANZESE, S. V. BULDYREV, H. J. HERRMANN, and H. E. STANLEY, *J. Chem. Phys.* **138**, 244506 (2013).
- [25] E. LASCARIS, T. A. KESSELRING, G. FRANZESE, S. V. BULDYREV, H. J. HERRMANN, and H. E. STANLEY, Response functions near the liquid-liquid critical point of ST2 water, in *4th International Symposium on Slow Dynamics in Complex Systems*, edited by M. TOKUYAMA and I. OPPENHEIMER, volume 1518, pp. 520–526, AIP Conf. Proc., 2013.
- [26] V. MOLINERO, S. SASTRY, and C. A. ANGELL, *Phys. Rev. Lett.* **97**, 075701 (2006).
- [27] F. H. STILLINGER and T. A. WEBER, *Phys. Rev. B* **31**, 5262 (1985).
- [28] V. V. VASISHT, S. SAW, and S. SASTRY, *Nature Phys.* **7**, 549 (2011).
- [29] V. KAPKO, private communication, 2013.
- [30] Y. TU, S. V. BULDYREV, Z. LIU, H. FANG, and H. E. STANLEY, *EPL* **97**, 56005 (2012).
- [31] J. R. ERRINGTON and P. G. DEBENEDETTI, *Nature* **409**, 318 (2001).
- [32] S. CHATTERJEE and P. G. DEBENEDETTI, *J. Chem. Phys.* **124**, 154503 (2006).
- [33] C. A. ANGELL, P. H. POOLE, and M. HEMMATI, A New Interpretation of Liquid-Liquid Unmixing in Classical Alkali Silicate Glasses, in *Proc. 12th East European Glass Conf. (Varna, Bulgaria)*, edited by B. SAMUNOVA and Y. DEMETRIEW, pp. 100–109, 1996.
- [34] R. J. CHARLES, *J. Am. Ceram. Soc.* **49**, 55 (1966).
- [35] R. J. CHARLES, *J. Am. Ceram. Soc.* **50**, 631 (1967).
- [36] R. J. CHARLES, *Phys. Chem. Glasses* **10**, 169 (1969).
- [37] F. Y. GALAKHOV and B. G. VARSHAL, Causes of phase separation in simple silicate systems, in *Phase-Separation Phenomena in Glasses*, edited by E. A. PORAI-KOSHITS, volume 8 of *The Structure of Glass*, pp. 7–11, Consultants Bureau, New York, 1973.
- [38] R. H. DOREMUS, *Glass Science*, Wiley, New York, 1973.
- [39] W. HALLER, D. H. BLACKBURN, and J. H. SIMMONS, *J. Am. Ceram. Soc.* **57**, 120 (1974).
- [40] M. MORISHITA, A. NAVROTSKY, and M. C. WILDING, *J. Am. Ceram. Soc.* **87**, 1550 (2004).
- [41] M. HEMMATI and C. A. ANGELL, *J. Non-Cryst. Solids* **217**, 236 (1997).